# The heterogeneous coma of comet 67P/Churyumov-Gerasimenko as seen by ROSINA: H2O, CO2, and CO from September 2014 to February 2016

M. Hoang, K. Altwegg, H. Balsiger, A. Beth, A. Bieler, U. Calmonte, M. R. Combi, J. de Keyser, B. Fiethe, N. Fougere, et al.

A&A 600, A77 (2017)
DOI: 10.1051/0004-6361/201629900


Astronomy & Astrophysics

# The heterogeneous coma of comet 67P/Churyumov-Gerasimenko as seen by ROSINA: $H_2O$, $CO_2$, and CO from September 2014 to February 2016

M. Hoang[1,2], K. Altwegg[3], H. Balsiger[3], A. Beth[4], A. Bieler[3,5], U. Calmonte[3], M. R. Combi[5], J. De Keyser[6], B. Fiethe[7], N. Fougere[5], S. A. Fuselier[8,9], A. Galli[3], P. Garnier[1,2], S. Gasc[3], T. Gombosi[5], K. C. Hansen[5], A. Jäckel[3], A. Korth[10], J. Lasue[1,2], L. Le Roy[3], U. Mall[10], H. Rème[1,2], M. Rubin[3], T. Sémon[3], D. Toublanc[1,2], C.-Y. Tzou[3], J. H. Waite[8], and P. Wurz[3]

[1] University of Toulouse, UPS-OMP, IRAP, 31400 Toulouse, France
e-mail: margaux.hoang@irap.omp.eu
[2] CNRS, IRAP, 9 avenue colonel Roche, BP 44346, 31028 Toulouse Cedex 4, France
[3] University of Bern, Physikalisches Institut, 3012 Bern, Switzerland
[4] Department of Physics, Imperial College London, London SW7 2AZ, UK
[5] University of Michigan, Department of Atmospheric Oceanic and Space Science, Ann Arbor, MI 48109, USA
[6] Royal Belgian Institute for Space Aeronomy (BIRA-IASB), 1180 Brussels, Belgium
[7] Technical University of Braunschweig, 38106 Braunschweig, Germany
[8] Southwest Research Institute, San Antonio, TX 78238, USA
[9] Department of Physics and Astronomy, University of Texas at San Antonio, San Antonio, Texas, TX 78249, USA
[10] Max-Planck Institute für Sonnensystemforschung, 37077 Göttingen, Germany

Received 14 October 2016 / Accepted 3 February 2017

**ABSTRACT**

*Context.* The ESA Rosetta mission has been investigating the environment of comet 67P/Churyumov-Gerasimenko (67P) since August 2014. Among the experiments on board the spacecraft, the ROSINA experiment (Rosetta Orbiter Spectrometer for Ion and Neutral Analysis) includes two mass spectrometers to analyse the composition of neutrals and ions and a COmet Pressure Sensor (COPS) to monitor the density and velocity of neutrals in the coma.
*Aims.* We study heterogeneities in the coma during three periods starting in October 2014 (summer in the northern hemisphere) and ending in February 2016 (end of winter in the northern hemisphere). We provide a detailed description of the main volatiles dynamics ($H_2O$, $CO_2$, CO) and their abundance ratios.
*Methods.* We analysed and compared the data of the Reflectron-type Time-Of-Flight (RTOF) mass spectrometer with data from both the Double Focusing Mass Spectrometer (DFMS) and COPS during the comet escort phase. This comparison has demonstrated that the observations performed with each ROSINA sensor are indeed consistent. Furthermore, we used a Direct Simulation Monte Carlo (DSMC) model to compare modelled densitites with in situ detections.
*Results.* Our analysis shows how the active regions of the main volatiles evolve with the seasons with a variability mostly driven by the illumination conditions; this is the case except for an unexpected dichotomy suggesting the presence of a dust layer containing water deposited in the northern hemisphere during previous perihelions hiding the presence of $CO_2$. The influence of various parameters is investigated in detail: distance to the comet, heliocentric distance, longitude and latitude of sub-satellite point, local time, and phase angle.

**Key words.** comets: individual: 67P/Churyumov-Gerasimenko – comets: general – planets and satellites: atmospheres

## 1. Introduction

After 10 years of travel, the Rosetta spacecraft arrived at comet 67P/Churyumov-Gerasimenko (67P) in August 2014 and started to study the weakly active nucleus with its onboard instruments. The spacecraft escorted the comet through its perihelion in August 2015 at 1.24 AU from the Sun. After 20 months of study, Rosetta recorded a large amount of in situ data and helped us to understand the composition and evolution of the coma of the comet along its orbit. Among the onboard instruments, the Rosetta Orbiter Spectrometer for Ion and Neutral Analysis (ROSINA) produced important results. We owe these results to the data from its two mass spectrometers, the Reflectron-type Time-Of-Flight (RTOF) mass spectrometer and the Double Focusing Mass Spectrometer (DFMS), and to data from the COmet Pressure Sensor (COPS). All three sensors are commonly operated through a data processing unit (DPU). RTOF has a wide mass range and a high temporal resolution (Scherer et al. 2006), while DFMS has high mass resolution and sensitivity (Balsiger et al. 2007). Both sensors were designed to measure the composition of the cometary neutral gas along with cometary ions. The third instrument, COPS, measures total density and bulk velocity of the gas (Balsiger et al. 2007).

A strong chemical heterogeneity in the coma during the summer in the northern hemisphere was revealed using the DFMS data by Hässig et al. (2015). These authors studied $H_2O$, $CO_2$, and CO variations in the coma and found diurnal and latitudinal

variations of $H_2O$ with a more homogeneous behaviour of $CO_2$ and CO, which probably originated from deeper layers inside the comet, whose rotation axis is tilted by 52 deg relative to its orbit. A high $CO_2/H_2O$ ratio ($\geqslant$2) region was located in the southern part of the bigger lobe, whereas the highest water densities were observed when the spacecraft was located above the neck area. Temporal variations of $H_2O$, $CO_2$, and CO seen by RTOF between 3.1 and 2.3 AU were given in Mall et al. (2016). Luspay-Kuti et al. (2015) demonstrated that minor species density variations are correlated with major species $H_2O$ or $CO_2$ while $CH_4$ shows a different pattern. Bieler et al. (2015) compared the three different models, purely geometrical, hydrodynamic, and Direct Simulation Monte Carlo (DSMC), and reproduced COPS data. Fougere et al. (2016) used DSMC model to fit DFMS measurements, when assuming that the activity of the comet is largely driven by solar illumination, including areas of higher activity.

Important results about the coma of 67P were also obtained from other instruments on board Rosetta, such as the ultraviolet imaging spectrometer called ALICE, with measurements of near-nucleus atomic hydrogen and oxygen emissions. These revealed an unexpected influence of electrons, rather than photons, on the break up of molecules (Feldman et al. 2015). Biver et al. (2015) also published a map of water vapour in the coma of 67P based on the Microwave Instrument for the Rosetta Orbiter data (MIRO), showing a very inhomogeneous distribution of water in the coma with the highest density above the active neck region. The active zones, such as the neck region, related to cliffs and pits – possibly due to sink-hole collapse – were mapped and discussed by Vincent et al. (2015, 2016) with the OSIRIS experiment (Optical, Spectroscopic, and Infra-red Remote Imaging System). The VIRTIS (Visible and InfraRed Thermal Imaging Spectrometer) team detailed the dynamics of 67P surface properties and the loss of a dust layer due to increased water sublimation during the approach to the Sun (Filacchione et al. 2016). They also revealed a cyclic pattern, which modifies the activity and water ice production rate on the surface of the comet (De Sanctis et al. 2015).

In this paper, we focus on the spatial and temporal variation of the densities of the main volatile species $H_2O$, $CO_2$, and CO provided by the RTOF instrument. The characterization of water and carbonic molecules in the coma is essential to understand the structure of cometary nuclei and thus the composition of the primordial solar system. We first describe the RTOF instrument briefly (further details are given by Gasc 2015). Then, we show that the density and dynamics of the main volatiles are complex and depend on several parameters such as comet-spacecraft distance, Sun-comet distance, the longitude and latitude of the sub-satellite point, and phase angle. A mapping of the coma reveals a heterogeneous seasonal production at the surface and a significant temporal variability correlated with heliocentric distance.

## 2. Description of the instruments and datasets

### 2.1. Description of the instruments

The RTOF mass spectrometer was designed to measure cometary neutral gas and cometary ions and, in particular, is able to detect heavy organic molecules with a very good mass resolution ($m/\Delta m$ = 500 at 50% level). This spectrometer is able to detect ions and molecules from 1 amu/e to 300 amu/e and has a high temporal resolution of 200 s (Scherer et al. 2006; Balsiger et al. 2007).

Spectra from the RTOF are recorded as abundance versus time of flight. To convert those spectra into abundance versus mass to charge ratio, a mass calibration is applied on each RTOF spectrum (Gasc et al. 2017). The instrument can be operated in different modes. In one of them, RTOF uses a gas calibration unit (GCU) to record spectra for mass calibration. The unit contains a well-calibrated gas mixture with helium, carbon dioxide, and krypton.

**Table 1.** Description of RTOF neutral modes used in this work.

| Mode | SS M0521 | OS M0524 |
|---|---|---|
| Extraction frequency | 10 kHz | 10 kHz |
| Filament emission | 200 $\mu$A | 200 $\mu$A |
| Acquisition time | 200 s | 400 s |

**Notes.** See Gasc et al. (2017) for further details.

The RTOF is actually two mass spectrometers in one instrument, each with its own ion source and detector optimized for different measurements. The channel with electron impact storage ions source or storage source (SS) samples the neutral gas, while the orthogonal extraction ion source channel or orthogonal source (OS) analyses cometary ions but can also measure neutral gas. These two channels are never used at the same time owing to power, data rate, and DPU data compression considerations. When cometary neutral gas enters, it is ionized by one of the ion sources. The charged particles are extracted towards the drift tube at a frequency of 2 kHz, 5 kHz, or 10 kHz. These particles finally reach a detector, which records the time of flight of each molecule that is proportional to the square root of the mass of the species. In this paper, the RTOF data discussed are signatures of volatiles detected with the SS M0521 and OS M0524 mode (see Table 1).

A typical spectrum recorded in SS mode is shown in Fig. 1 with $H_2O$ (mass 18.01 u/e), CO (mass 27.99 u/e), and $CO_2$ (mass 43.98 u/e).

Analysis of the data was performed with the Spectra Analyser software developed and provided by S. Gasc for mass scaling, peaks fitting, and temporal evolution analysing. Using GCU mode, a defined quantity of a gas mixture is introduced into the ion source that can be used to calibrate the time-of-flight spectra into mass to charge scale. The fitting method, which is based on a pseudo-Voigt function, takes background, offset, and electronic noise into account. This method gives us a molecule abundance per 200 or 400 s for each mass depending on the mode. We then convert abundance [counts/s] into density [$cm^{-3}$]. The method used is explained in Gasc et al. (2017). The $CO_2/H_2O$ and $CO/H_2O$ ratios are calculated for each spectrum provided by RTOF.

The DFMS is a high mass resolution ($m/\Delta m$ = 3000 at 1% level) and high sensitivity mass spectrometer with a mass range of 1–150 amu that is designed to measure the composition of the cometary neutral gas and cometary ions (Balsiger et al. 2007). The gas is first ionized in the instrument by electron impact. The mass analyser is a combination of a 90 deg deflection electrostatic analyser and a 60 deg deflection magnetic analyser. A mass scan is achieved mass-by-mass by varying the sensor potentials. The integration time per mass is 20 s, leading to a lower temporal resolution for each species than for RTOF (e.g. about 40 min for $H_2O$).

The COPS instrument consists of two separate sensors, i.e. the nude gauge (NG) and the ram gauge (RG). The NG measures in situ the total ambient neutral number density (with no separation between the species), whereas the RG measures the ram pressure of the expanding cometary atmosphere.

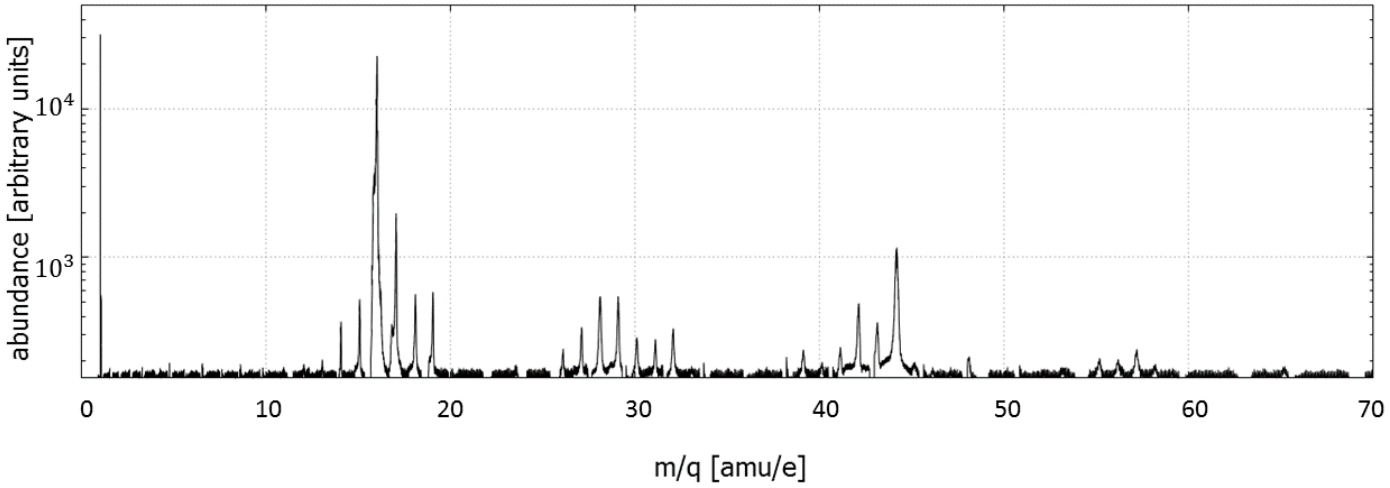


**Fig. 1.** Typical RTOF spectrum recorded in storage source (SS) mode showing $H_2O$ (mass 18.01 u/e), CO (mass 27.99 u/e), $CO_2$ (mass 43.98 u/e), and their fragments.

In this paper, we used COPS nude gauge data, which were calibrated using the following processes. First, we removed the background density ($1.2 \times 10^6$ cm$^{-3}$, which corresponds to $5 \times 10^{-11}$ mbar at 293 Kelvin). Second, sharp neutral density peaks are seen by COPS when thrusters are fired during spacecraft maneuvers or wheel off-loadings or when the spacecraft changes orientation, where cold parts of the spacecraft previously in shadow may get illuminated by the Sun. Thus, COPS nude gauge data acquired during a maneuver or when the nadir off-pointing angle is greater than 5 deg are ignored. Lastly, a correction is applied of COPS neutral density to the sensitivity of different gas species using relative abundances from either RTOF or DFMS.

To compare RTOF and DFMS data, we have to take into account the specific sensitivity and fragmentation pattern of each species and mode, which are different for both instruments.

Densities of $H_2O$, $CO_2$, and CO are calculated via the equations below, which derive the relative abundances from the mass spectrometers and scale the results to the COPS total densities (Gasc et al. 2017), as follows:

$$n_{H_2O} = \frac{n_{COPS}}{\left(\frac{1}{\beta_{H_2O}} + \frac{r_{CO}}{\beta_{CO}} + \frac{r_{CO_2}}{\beta_{CO_2}}\right)}$$

$$n_{CO_2} = r_{CO_2}.n_{H_2O}$$

$$n_{CO} = r_{CO}.n_{H_2O},$$

where $n_i$ are specific densities in [cm$^{-3}$], $\beta_i$ are scale factors relative to $N_2$, and $r_i$ are ratios of the densities relative to $H_2O$.

The $CO_2/H_2O$ and $CO/H_2O$ ratios needed to obtain the volatiles densities are defined as

$$r_{CO_2} = \frac{c_{CO_2}}{c_{H_2O}}.\frac{S_{H_2O}}{S_{CO_2}}.\frac{f_{H_2O\to H_2O}}{f_{CO_2\to CO_2}}$$

$$r_{CO} = \frac{c_{CO}}{c_{H_2O}}.\frac{S_{H_2O}}{S_{CO}}.\frac{f_{H_2O\to H_2O}}{f_{CO\to CO}} - r_{CO_2}.f_{CO_2\to CO},$$

where $c_i$ is the number of detections within 200 or 400 s, $S_i$ is the species; sensor and emission dependent sensitivity; and $f_{i\to j}$ is the relative fragmentation or isotopic ratio, where $i$ is the parent and $j$ one of the fragments

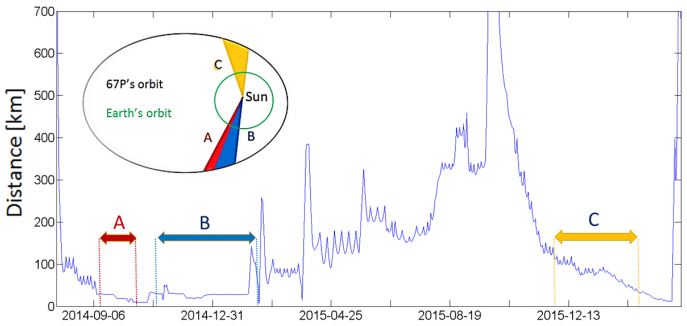


**Fig. 2.** Evolution of the distance between the spacecraft and 67P. Studied periods: period A, from 10 September to 30 October 2014; period B, from 1 November 2014 to 15 February 2015; and period C, from 1 December 2015 to 15 February 2016.

### 2.2. Description of the datasets

The data were analysed for three periods. During those periods, Rosetta observed almost the entire surface of the comet, whose rotation period is 12.4 h (Sierks et al. 2015) and covered heliocentric distances from 3.45 to 1.2 AU (see Fig. 2). The other periods could not be included in this study because of their low signal-to-noise ratio (essentially when the spacecraft was at large distances).

The first studied period started on 10 September 2014 and ended on 30 October 2014. The distance between Rosetta and 67P decreased from 30 km to 10 km and allowed a first close approach to the comet. During period A, the heliocentric distance decreased from 3.45 to 3.05 AU, and RTOF recorded almost 15 000 spectra in SS mode (2100 measurements for DFMS).

The second period followed the first closely. It started on 1 November 2014 and ended on 1 February 2015. During this period, the sublimation of water highly increased and became strong in places where the solar irradiation heated the cometary surface sufficiently. At the beginning of this period, the heliocentric distance was 3.05 AU and the estimated production rate was $2 \times 10^5$ kg per day. It reached $7 \times 10^5$ kg per day at the end of the period, around 2.4 AU (Hansen et al. 2016). The data from the second period were taken in OS mode. The spacecraft orbited the comet at an altitude of about 20 km during the majority of this period except in mid-November 2014 with a fly-by at 16 km

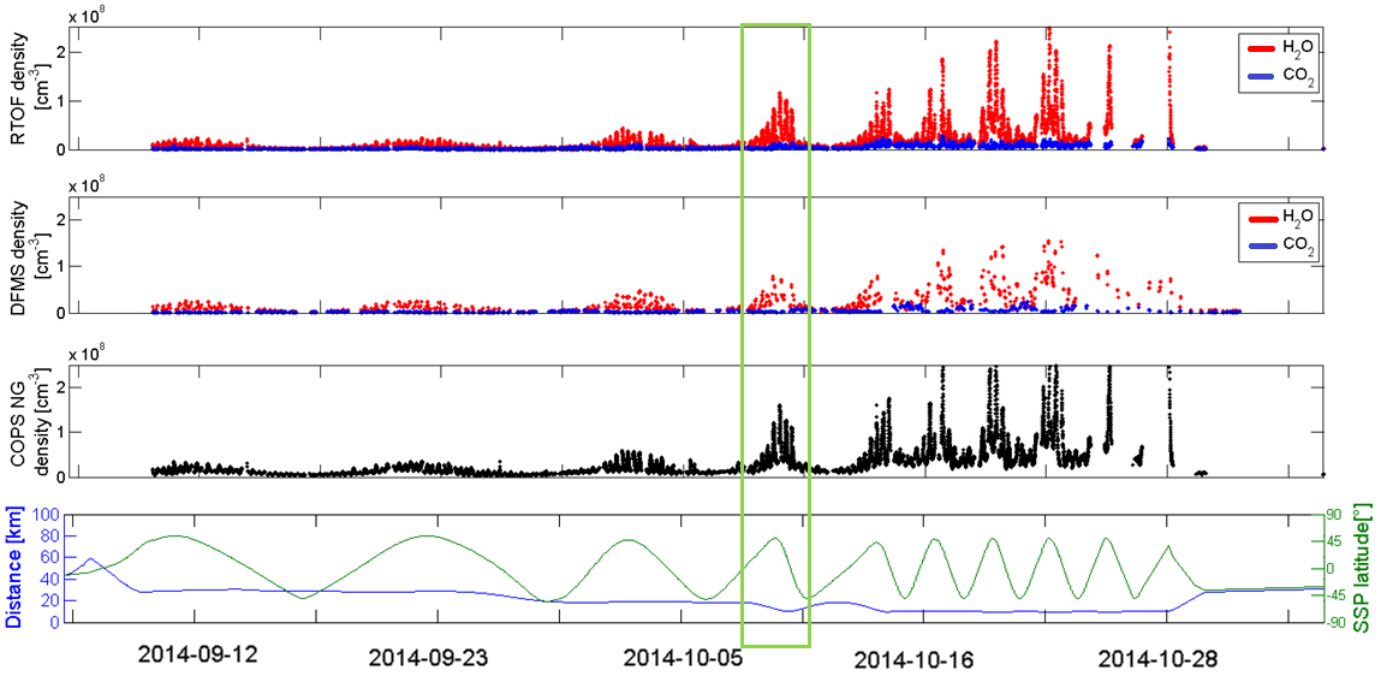


**Fig. 3.** Measured densities for $H_2O$ (in red) and $CO_2$ (in blue) by RTOF (*upper panel*) and DFMS (*second panel*) for period A. *Third panel*: COPS total density from the nude gauge. The *lower panel* provides the variation of the distance between the comet and the spacecraft in blue and the variation of the sub-satellite point latitude in green. A zoom of the green rectangle area is shown in the next figure.

for Philae's landing. The phase angle, i.e. the angle between the spacecraft and Sun directions from the centre of the comet, was also roughly stable near 90°.

The third studied period occurred after first equinox (10 May 2015) started on 1 December 2015 (1.8 AU) and ended on 15 February 2016 (2.2 AU). The northern hemisphere (encountering summer during period A and B became the winter hemisphere and this changed the active regions considerably. During those months, the spacecraft slowly came closer to the comet from an initial distance of 100 kilometers to a distance of about 38 km in the end of period C.

## 3. Results

### 3.1. Temporal variation

The search for gas production heterogeneities at the nucleus surface is required to associate the coma measurements with source locations at the surface, assuming a radial outflow as a first step. Owing to the irregular shape of 67P, the flow is not radial very close to the nucleus, but the flow becomes closer to a straight line as the gas expands away from the nucleus (see Fig. A.1). The field of view is 10° × 40° for RTOF and 20° × 20° for DFMS. We thus associated each detection with the corresponding sub-satellite point (SSP) in latitude and longitude in a frame centred on and rotating with the comet. Latitude 0° separates the comet in two hemispheres and when the spacecraft points to the extremity of the head of the comet, the SSP position corresponds to (0°, 0°). In this section, we describe the temporal variability of the main volatiles densities and progressively discuss the various parameters of influence.

#### 3.1.1. Period A

The first period is used to study the RTOF and DFMS temporal variations for $H_2O$, CO, and $CO_2$ and compare the total density with COPS measurements. We then highlight the influence of different parameters (distance to comet and sub-satellite latitude and longitude).

Once the density of the main volatiles is deduced from the spectra, we can visualize the temporal evolution as in Fig. 3. All the spectra show a clear signature of $H_2O$, $CO_2$, and CO. In RTOF spectra, the $H_2O$ peak is almost always higher than the $CO_2$ and CO peaks. CO detections are not visible in the RTOF panel; they are very close to $CO_2$ detections during period A (see Fig. 4). Nevertheless, $CO_2$ may exceed the $H_2O$ detection, in particular, in the southern hemisphere (see Sect. 3.2 along with the early results by Mall et al. 2016; and Hässig et al. 2015). The COPS data, in the middle panel, show the global variation of the total gas density that reaches the spacecraft.

The global periodic pattern is well known on 67P with a clear and strong diurnal variation. $H_2O$ densities in particular followed closely the variation of the sub-satellite point latitude. The northern hemisphere was well illuminated during this period and this led to enhanced sublimation for positive latitude regions. The diurnal variation seen in RTOF and DFMS data is well confirmed by COPS. The difference of temporal resolution can be seen in the set of data of the two spectrometers: DFMS recorded less data. The maxima of periodic variations appeared lower than in the RTOF panel.

As Rosetta came closer to the comet, the ROSINA instruments recorded a progressive increase of density with a maximum when the spacecraft reached 10 kilometers.

The variation of the sub-satellite point longitude also impacted the detection of volatiles, as found in the high frequency variations, shown in Fig. 4. For one comet rotation, we observe for $H_2O$ two minima (1 and 3 on upper panel) and two maxima (2 and 4) directly correlated with the longitude variations and the geometrical asymmetry of 67P. The $CO_2$ and CO observations showed more complex density variations with detections in both hemispheres and less clear asymmetries (see also Hässig et al. 2015), as discussed further in Sect. 3. A

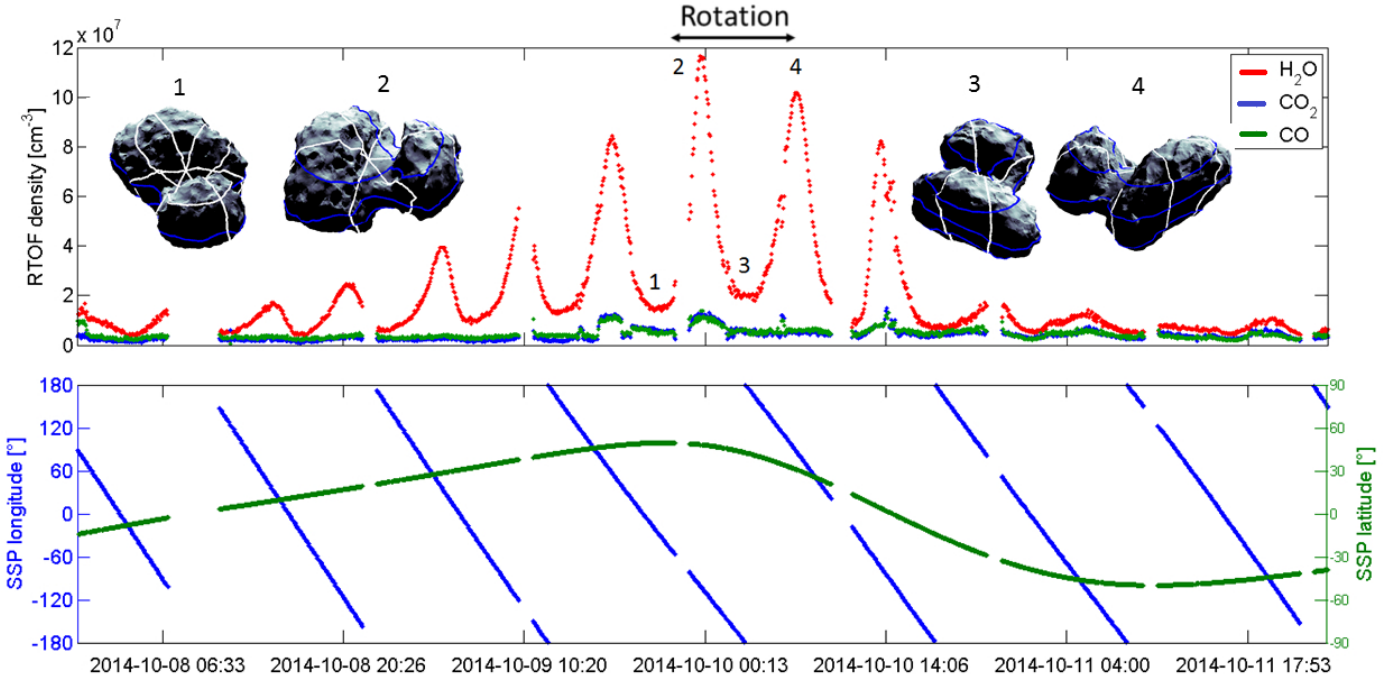


**Fig. 4.** Diurnal variation of main volatiles. *Upper panel*: zoom of upper panel of Fig. 3 from 8 October to 11 October with the view of the comet from the spacecraft at specific times. *Lower panel*: sub-satellite point longitude and latitude variations during the same period.

Lomb-Scargle periodogram (not shown) was applied to $H_2O$ data to highlight periodic signals on a statistical basis and confirmed the presence of strong periodicities of about 6 and 12 h. These periodic variations are linked to the geometry of the nucleus. When SSP $= (90°, 0°)$, the spacecraft sees a large illuminated area that includes the active neck region. Since the rotation period of 67P was about 12.4 h at that time in the mission, this induces a half-diurnal variation for coma measurements with high detections each time the spacecraft is above the neck, i.e. approximately every 6.2 h. Lomb-Scargle periodograms applied to $CO_2$ and CO data showed a more homogeneous behaviour with a smaller 12 h periodicity; this confirmed that carbon dioxide and monoxide are more uniformly distributed than water in the top layer of the comet, as we can also see through the analysis of short time periods, following the results of Hässig et al. (2015). This behaviour of the main volatiles is in agreement with the common assumption that $CO_2$ and CO originates from deeper layers than $H_2O$ (De Sanctis et al. 2010; Prialnik et al. 2004). This can be interpreted as the water sublimation is occurring from the shallow subsurface, which is very sensitive to diurnal temperature variations, while $CO_2$ and CO sublimate from deeper layers inside the comet that are also influenced by a seasonal effect due to obliquity in agreement with thermodynamic models of the cometary subsurface (Huebner et al. 2006; De Sanctis et al. 2010).

A similar behaviour was detected by the Deep Impact spacecraft at comet 103P/Hartley 2, where the water release was mostly originating from the illuminated part of the nucleus (A'Hearn et al. 2011).

### 3.1.2. Period B

In Fig. 5, we show the temporal variation of $H_2O$, in red, and $CO_2$, in blue, obtained with the period B spectra.

Beyond the sources of variability discussed above, the composition and dynamics of the coma as measured by ROSINA also depend on parameters such as the phase angle and nadir off-pointing. The phase angle was mostly constant near 90°, except at two times (start and end of period B) when it dropped significantly, leading to enhanced densities as expected (for a solar driven outgassing). Most of the variations observed in the nadir off-pointing are due to unavoidable spacecraft maneuvers that are necessary for navigation purposes or requested by other scanning instruments, such as ALICE or VIRTIS. We therefore applied a data filtering to ignore the detections when the amplitude of a slew exceeds 5°, considering that the instruments are not pointing to the comet anymore.

The second panel of Fig. 5 shows the $H_2O$ and $CO_2$ densities derived from the DSMC model detailed in Bieler et al. (2015) and Fougere et al. (2016). For a given illumination, this model reproduces the collisions and trajectories of the particles from the surface to the spacecraft (including a heterogeneous activity map; see Fougere et al. 2016), allowing us to link the surface processes and the in situ reference data recorded by ROSINA. The DSMC model was successfully compared with both COPS and DFMS data. It is now also clear that it can correctly reproduce the RTOF in situ measurements (up to perihelion at least). A more detailed analysis reveals that the DSMC model reproduces well the RTOF $H_2O$ and $CO_2$ variabilities except during period A (see Fig. A.2), where the DSMC model underestimates/overestimates the $CO_2$ density in the northern/southern hemisphere. The data are less correlated during Period A since DSMC model needs large periods of time to retrieve activity maps and $CO_2$ active areas may be unstable (Filaccione et al. 2016; see also the evolution of our maps from period A to B). For Period B, the ratio between the DSMC model and RTOF $H_2O$ and $CO_2$ is stable around one, corresponding to a good agreement for both species.

Except during the first 15 days of November 2014, with the approach and landing of Philae, the density of $H_2O$ accurately followed the variation of the sub-satellite point latitude. As during period A, higher water densities were measured when

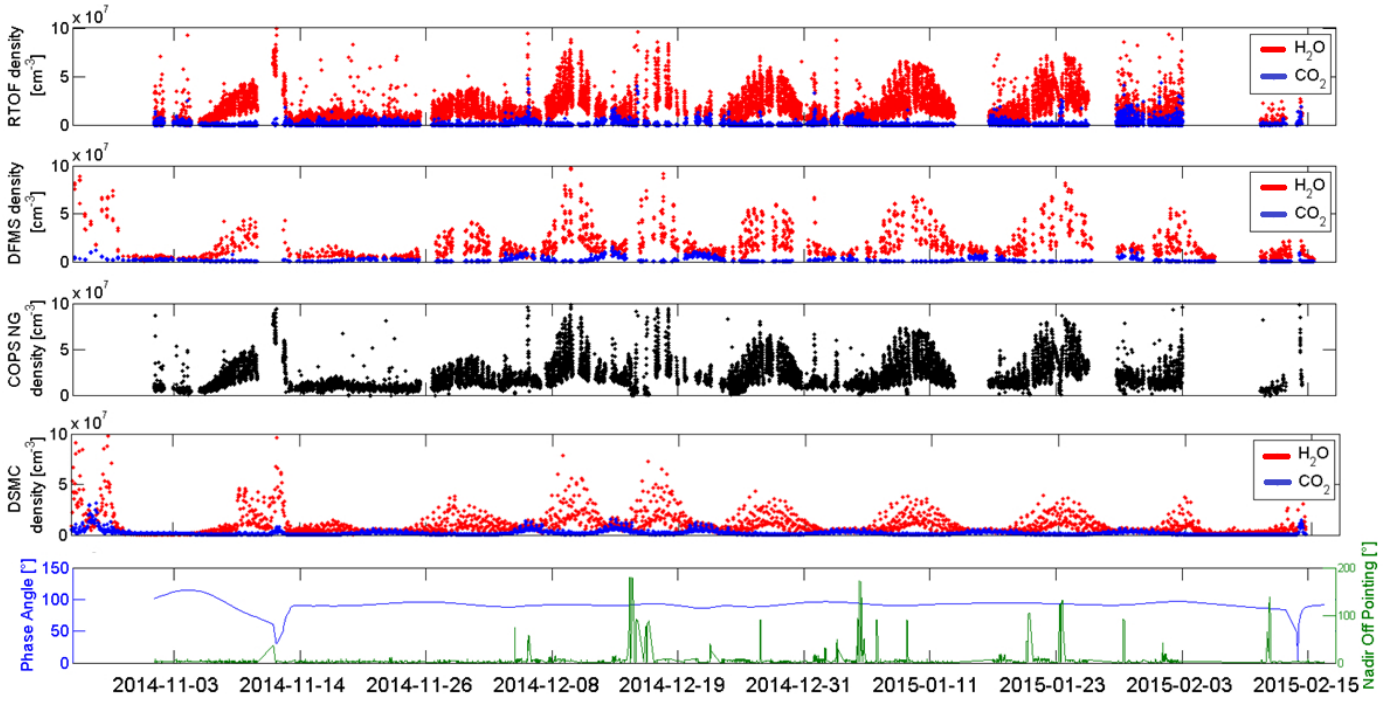


**Fig. 5.** Temporal evolution of $H_2O$ and $CO_2$ densities detected by RTOF (*upper panel*) and DFMS (*second panel*) during period B. *Third panel*: COPS nude gauge total densities. *Fourth panel*: $H_2O$ and $CO_2$ densities derived from the DSMC model (Bieler et al. 2015; Fougere et al. 2016). *Lower panel*: phase-angle variations in blue and nadir off-pointing angle variations in green.

the instrument was above the neck region in the northern hemisphere.

The largest $CO_2$ and CO densities correspond here to negative latitudes (southern hemisphere), whereas the situation was more complex during period A in which $CO_2$ and CO were also detected in the northern hemisphere (see Sect. 3.2 for detailed maps). As seen around 5 December 2014, 13 December 2014, and 3 January 2015 (Fig. 5; panels 1, 2 and 3), maximum $CO_2$ measurements appeared at minimum $H_2O$ detections.

Figure 6 provides the temporal variations of $CO/H_2O$ and $CO_2/H_2O$ ratios from RTOF and DFMS compared with the latitude of the sub-satellite point. The correlation between the RTOF and DFMS ratios is very good, despite a significant dispersion of RTOF values partially due to the higher time resolution of RTOF; also, the anti-correlation between the ratio evolution and the variation of latitude during period B. CO and $CO_2$ were essentially detected from the southern hemisphere (see also Sect. 3.2).

#### 3.1.3. Period C

The RTOF switched between SS and OS modes regularly during period C. We studied 6300 SS spectra to plot the evolution of $H_2O$, CO, and $CO_2$ in the upper panel of Fig. 7 and the corresponding DFMS and COPS densities, which are well correlated with RTOF data when both datasets are available.

In period A and B, CO and $CO_2$ variations were roughly anti-correlated with $H_2O$, meaning that they originated from different hemispheres on the comet. In this third period, CO and $CO_2$ variations followed the $H_2O$ variations and seemed to be concentrated in the southern hemisphere. The total density variation also appears to be anti-correlated with the SSP latitude. As 67P passed the inbound equinox (May 2015), the illumination crossed the equator and moved to the southern hemisphere. After his first equinox, the maximum of sublimation came from negative latitudes. These observations are in agreement with the results from VIRTIS-H observations (Bockelée-Morvan et al. 2016) and from modelling (Fougere et al. 2016).

We studied the evolution of the $CO_2/H_2O$ and $CO/H_2O$ density ratios from RTOF and DFMS as a function of the distance to the Sun. The average trends from in situ measurements (with a more significant dispersion for the RTOF data) show a decrease in the ratios with decreasing distance to the Sun due to an enhanced $H_2O$ outgassing at closer distances to the Sun; this is in agreement with the Snodgrass et al. (2013) predictions of outgassing rates ratios.

### 3.2. Spatial variation

As demonstrated above, the temporal variations observed by Rosetta are induced by the combination of different parameters, i.e. mostly the distance to the comet, the spatial variations (related to either illumination or longitude/latitude), and the distance to the Sun that plays a role in long timescales. In this section, we specifically study the spatial variations. Consequently, we first need to eliminate the influence of the distance between the spacecraft and the comet: we normalized all the densities from RTOF and DFMS to expected densities at 10 km from the nucleus. Assuming that the comet is a point source with no significant loss process at such small distances, we use a $1/r^2$ law to estimate the normalized densities.

This power law approximation was first confirmed by Hässig et al. (2015) and we were able to verify this approximation based on the COPS density measurements obtained after the 15 February 2015 fly-by (with an altitude running from 8 to 242 km in only three days), which led to a power-law statistical fit with a slope in between –1.8 and –1.9.

After removing most of the influence of the distance to the comet, the major source of variability is obviously the spatial variation due to the illumination by the Sun (and the induced sublimation process). The solar illumination is however not the

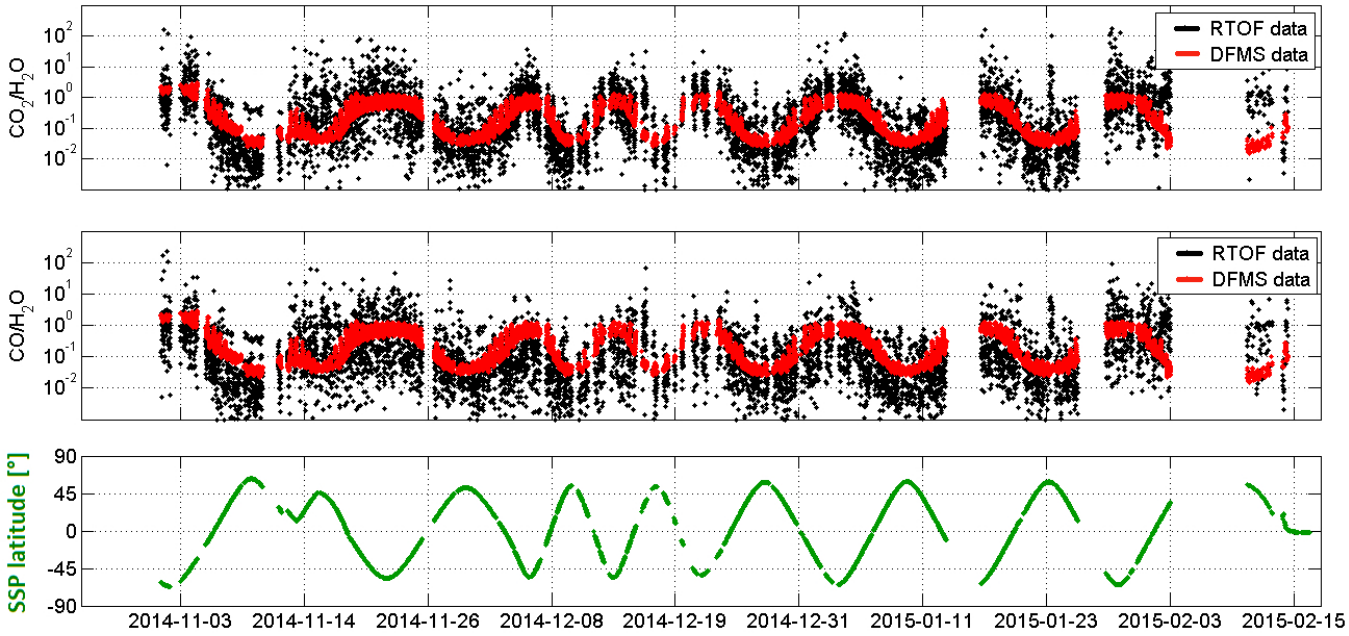


**Fig. 6.** $CO_2/H_2O$ and $CO/H_2O$ ratios from RTOF and DFMS compared with the latitude of the sub-satellite point (SSP) during period B.

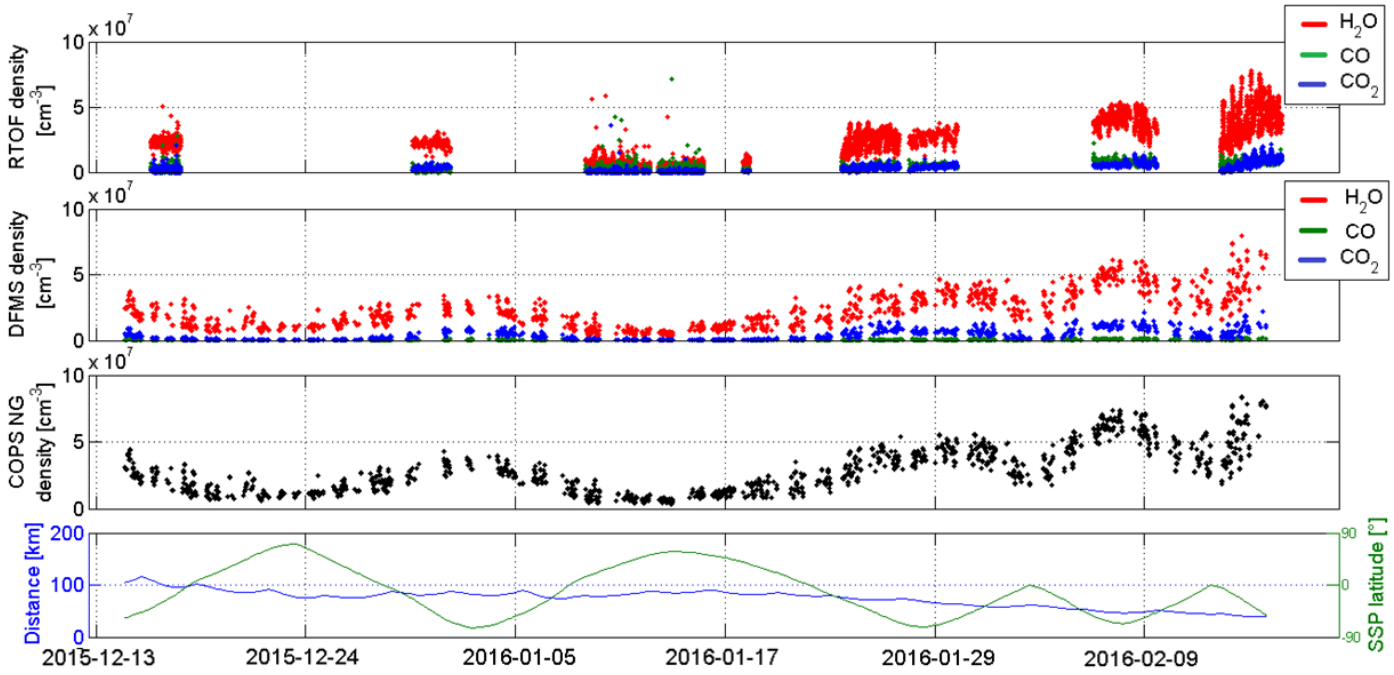


**Fig. 7.** Period C ROSINA data and orbitography. *Upper panel*: RTOF densities for $H_2O$ (in red), CO (in green), and $CO_2$ (in blue). *Second panel*: DFMS specific densities for $H_2O$ (in red), CO (in green), and $CO_2$ (in blue). *Third panel*, COPS NG total densities. *Lower panel*: variation of distance between comet and spacecraft (in blue) and variation of sub-satellite point latitude (in green).

only origin of spatial heterogeneities in the coma, there are also clear heterogeneities related to particular geographic regions (as mentioned for mostly pre-perihelion coma measurements in several studies; see Sect. 1).

To investigate the spatial heterogeneities at the surface of the comet, we created density maps using the density values normalized at 10 km distance and assuming that the recorded signal originates from the sub-spacecraft point. These maps are shown in the six lower panels in Fig. 8, showing the RTOF densities of $H_2O/CO_2/CO$ during the periods A/B/C. These are 2D maps in longitude/latitude with facets of 5 × 5 deg. The centre of each map represents the extremity of the head lobe, whereas the sides (+ or −180 deg) correspond to the Imhotep region on the big lobe. The correspondence between the morphological regions introduced by El-Maarry et al. (2015) and this 2D mapping is shown in Fig. A.3. Since most of the facets have been observed several times, each value associated with a facet is a mean value. Facets with less than 5 data points associated are coloured in white.

We use the SSP coordinates to project each RTOF measurement on the surface of the comet. We thus assume that the source region is located at the SSP. This is an important and simplifying

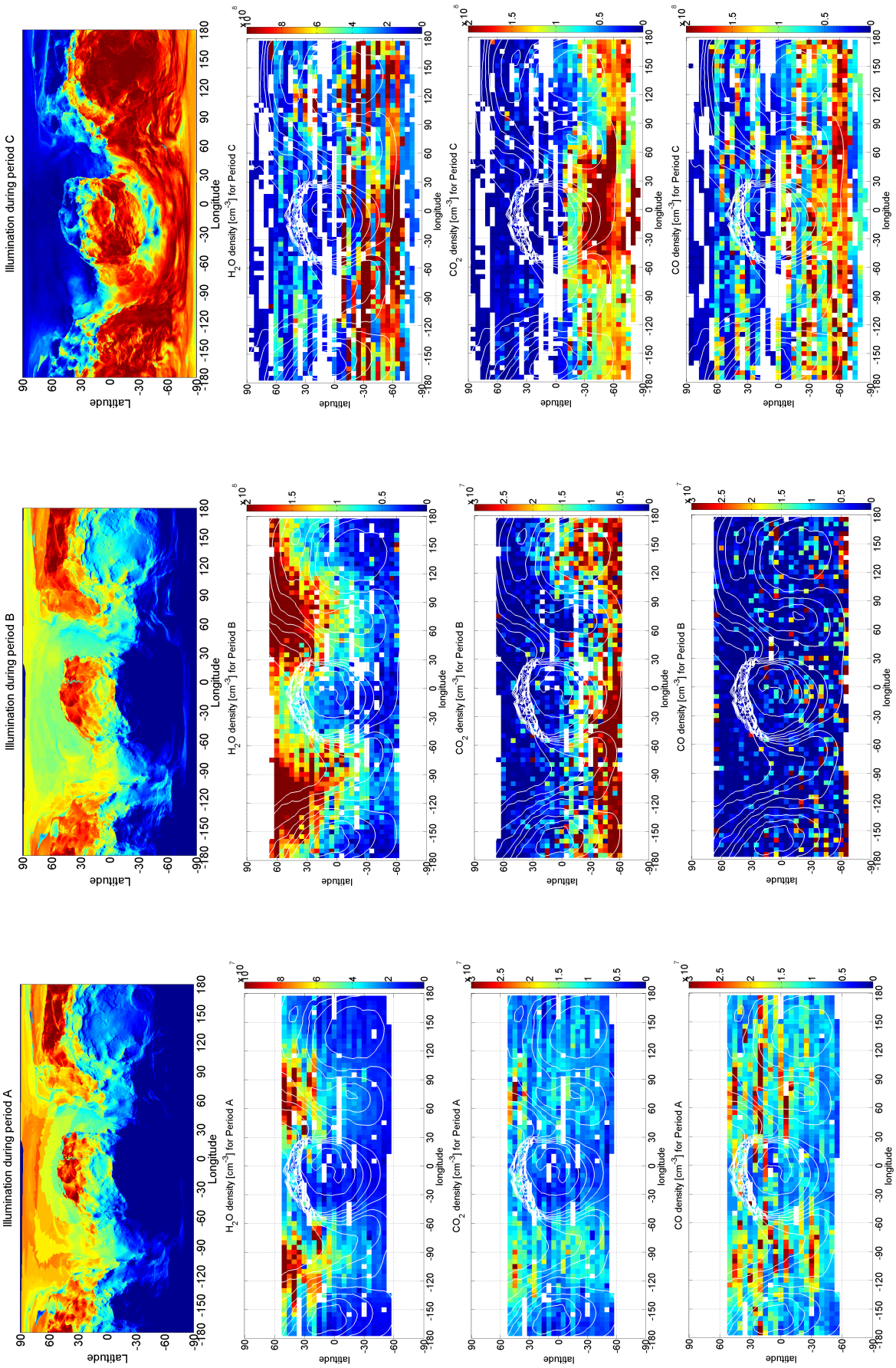


**Fig. 8.** Maps of illumination and densities. *Upper panels*: *left*, *middle*, and *right* figures represent 2D longitude/latitude maps of average illumination during periods A/B/C. The corresponding 2D maps of $H_2O$, $CO_2$, and CO densities in $cm^{-3}$ measured by RTOF (*the second, third and fourth rows*, respectively) normalized at 10 km with a $1/r^2$ scaling law, projected to the SSP longitude and latitude. The latitude 0 separates northern and southern hemispheres and topography lines;white contour lines in the maps are added on the 3D shape model provided by ESA/Rosetta/MPS for OSIRIS Team MPS/UPD/LAM/IAA/SSO/INTA/UPM/DASP/IDA.

assumption; since the comet shape is complex, the spacecraft is far from the comet, the comet is fully inside the RTOF field of view, and the outflow is not purely radial from the surface. Nevertheless, those steps allow us to understand the link between the main heterogeneities in the coma and the comet surface.

To study the correlation between solar illumination and outgassing, we produced three maps of illumination, corresponding to periods A, B, and C, based on an illumation code developed for 67P (by D. Toublanc, A. Beth). The normalized intensity of the colour (maxima in red, minima in blue) at every illuminated facet is given by the cosine of the angle between the surface normal and the direction to the Sun (average over one rotation period with mean latitude conditions appropriate to each period considered). The illumination maps of periods A and B are almost identical with the illuminated regions in the northern (summer) hemisphere, mostly the Set, Ash, Ma'at, and Hapi regions, extending towards slightly lower latitudes during the period B closer to equinox (with a larger total flux not seen because of the normalization). During period C, the southern (summer) hemisphere becomes strongly illuminated, except just below the head of the comet (Sobek region) that was in shadow.

During the three periods, the influence of illumination is clearly responsible for the $H_2O$ behaviour with a strong correlation between illuminated and active regions except for the small lobe of the comet, where fewer $H_2O$ detections are obtained. The $H_2O$ maps for periods A and B (upper left panels of Fig. 8) reveal an obvious and coherent inhomogeneous production. The production was very localized in the northern summer hemisphere around the neck zone with a maximum at the highest latitudes, where RTOF sometimes detected hundreds of counts per second. The illuminated neck zone thus appears responsible for the most important outgassing of water, as previously observed by several instruments (Biver et al. 2015; Hässig et al. 2015; Vincent et al. 2015). According to the analysis presented in Fig. 8, $H_2O$ essentially originates from the Babi, Hapi, and Seth regions (see Fig. A.3).

In the second period, the maps reveal an active northern hemisphere with wider source regions for water as the comet further approaches the Sun. $H_2O$ is predominant in the northern hemisphere before perihelion and was expected to be detected in the southern hemisphere after equinox in early May 2015, as shown and confirmed in the $H_2O$ map for period C.

The $CO_2$ map from period A shows that $CO_2$ detections were less abundant and more diffuse than water detections. CO also appeared less localized and showed a similar behaviour to $CO_2$. Both species were detected above both hemispheres, mostly above the neck region and above regions close to the head (Anubis, Anuket) or to the body (Babi, Aker, Khepri) as well as from the Imhotep region.

During period B, the $CO_2$ densities increased and appeared more localized. Most of the detections were obtained in the southern hemisphere (essentially below 30 deg latitude south, except for the Imhotep large source region), which was the less illuminated part of the comet during the studied period. The CO outgassing was even more diffuse than $CO_2$ with the largest values in the southern hemisphere as well.

During period C, in which the illumination was maximum in the southern hemisphere, $CO_2$ and CO kept approximately the same behaviour as during period B with maximum detections in the southern hemisphere. The source regions appeared diffuse (all the more for CO) with the largest sources located below the head of the comet and below the Imhotep region. We also investigated the ratios $CO_2/H_2O$ and $CO/H_2O$, which are important for understanding the coma and nucleus heterogeneities.

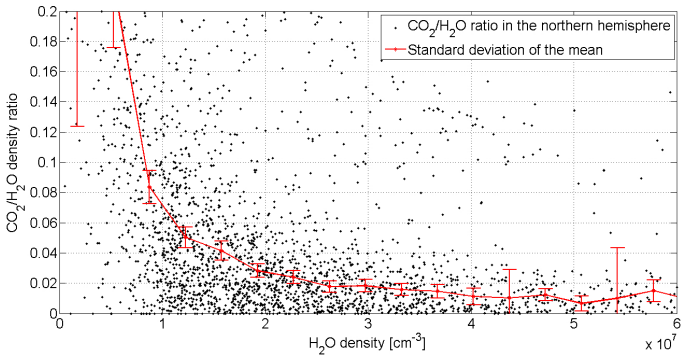


**Fig. 9.** $CO_2/H_2O$ density ratio from RTOF as a function of $H_2O$ density from 24 November 2014 to 24 January 2015. This figure is compared with the similar analysis in Fig. 11 of Bockelée-Morvan et al. (2015),which is also shown in Fig. A.1.

Overall $H_2O$ is dominant compared to $CO_2$ and CO, but ratios above unity were often seen, for example in the southern hemisphere during the northern summer season. Figure 9 shows the $CO_2/H_2O$ density ratio as a function of $H_2O$ density from RTOF, which can be compared with the same ratio (as a function of column density) as seen by the Visible InfraRed Thermal Imaging Spectrometer (VIRTIS; see Fig. A.4, taken from Bockelée-Morvan et al. 2015) during the exact same period. Despite the different techniques and instruments (in situ versus remote sensing), the results are strikingly similar with a clear anticorrelation between the $CO_2/H_2O$ ratio and $H_2O$ density or column density – in agreement with the previous conclusions on the period B – down to a minimum value of 0.01–0.02 in the northern hemisphere. We also observe some $CO_2$ coming from both illuminated and non-illuminated parts of the nucleus, as mentioned by Bockelée-Morvan et al. (2015).

Figure 10 provides the $CO_2/H_2O$ and $CO/H_2O$ ratios during period B from both RTOF and DFMS in a 2D mapping similar to Fig. 8. This allows us to both investigate the ratios above specific regions of 67P (beyond the comparisons between hemispheres previously discussed) and compare the results obtained by the two ROSINA spectrometers. The two spectrometers produce very similar maps for both $CO_2$ and CO ratios with a much larger number of points per cell (factor 7) for RTOF owing to the very different time resolution between the instruments. Overall, the highest ratios seen by both instruments were very localized in the southern hemisphere. More precisely, the $CO/H_2O$ ratio was highest (>0.3–0.4) in the Imhotep, Khonsu, Wosret, Neith, and Sobek regions, whereas the $CO_2/H_2O$ was highest (>0.5) in the same regions as $CO/H_2O$ but also in the whole latitude band [–60° –30°] (with parts of the Anhur, Bes, Atum, and Geb regions). The data do not allow us to provide conclusions on the regions below –60° latitude. The $CO/H_2O$ ratio appeared both overall more homogeneous and with the highest detections more confined to the southern parts of the head and body of the comet, whereas $CO_2$ was strongly confined to and spread over the southern hemisphere in agreement with the previous conclusions on the density maps of both species and the illumination conditions of period B. Beyond period B, the CO and $CO_2$ ratios decreased on average while getting closer to the Sun because of an increased water outgassing. Moreover, the mapping of ratios during period C (not shown) shows a much more homogeneous distribution, in agreement with the illumination of the southern hemisphere, which leads to the highest measured densities in all three species in the same hemisphere.

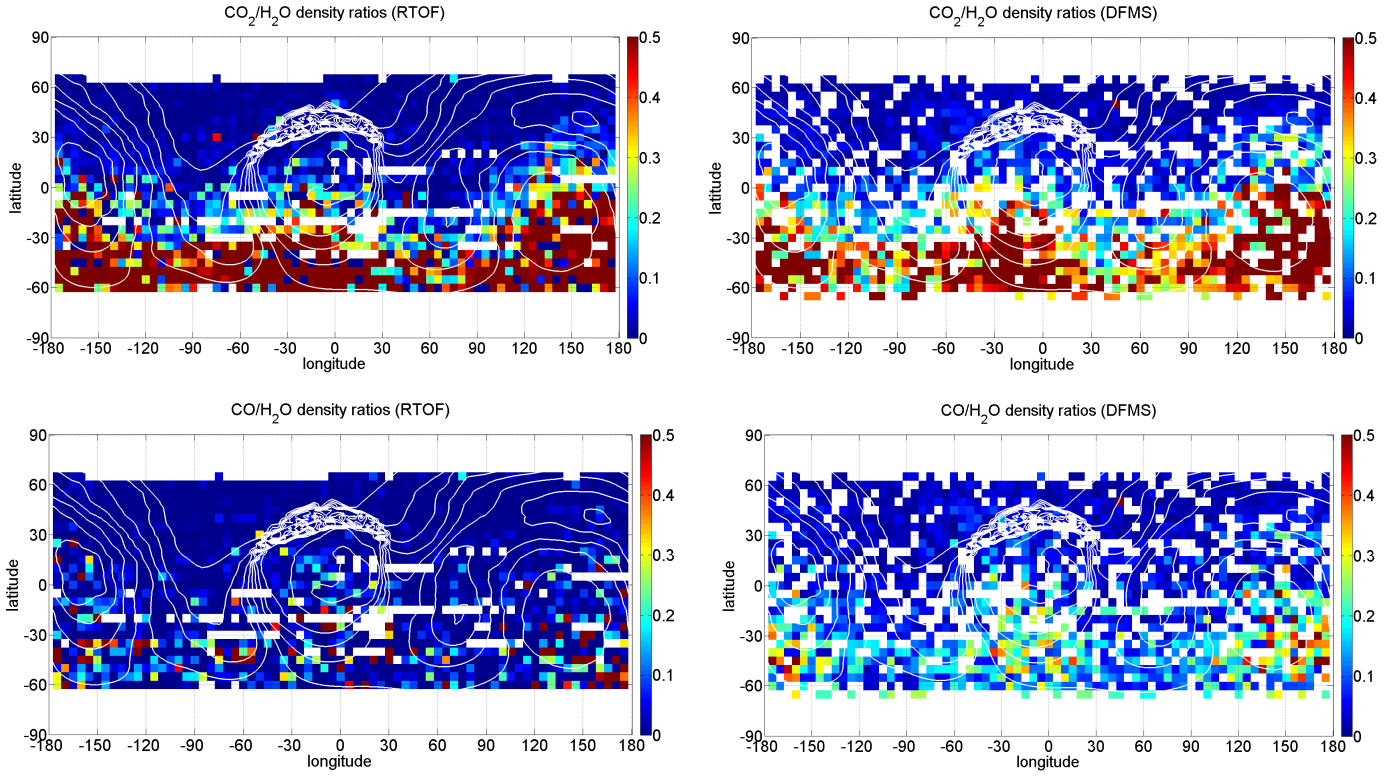


**Fig. 10.** Two-dimensional maps of $CO_2/H_2O$ (*upper panels*) and $CO/H_2O$ (*lower panels*) density ratios based on RTOF (*left*) and DFMS (*right*) data for period B.

### 3.2.1. Discussion

The observations about the respective production regions of $H_2O$, $CO_2$, and CO among the three periods are roughly in agreement with an illumination driven outgassing of the main volatiles. In particular, the observations during the periods A and B are in agreement with an illuminated northern hemisphere at 150–200 K allowing for increased $H_2O$ outgassing. This agrees with the conclusions provided by the VIRTIS team (Capaccioni et al. 2015), who obtained an illuminated surface temperature from 180 to 230 K, and the MIRO team, who determined a subsurface temperature of 160–180 K (Gulkis et al. 2015). The neck region was however by far the most active part of the northern hemisphere for $H_2O$, as known from earlier measurements (Luspay-Kuti et al. 2015; Lee et al. 2015). This region contains a large number of active pits (Vincent et al. 2015) and cliffs (Vincent et al. 2016), which combined with the higher temperature gradients (Alí-Lagoa et al. 2015), made it the most active region when illuminated during summer on the northern hemisphere. Another interpretation could also be that ejected icy grains were redeposited on the neck (owing to its gravitational well) and covered the northern hemisphere after the active period of the previous perihelion. We may add that $H_2O$ detections were almost absent above the northern part of the head (Ma'at region) despite strong illumination conditions. These conditions may be due to the dust coverage of this region (El-Maarry et al. 2015) with dust depleted in water ice, where the wet ice extracted from the southern hemisphere is preferentially deposited on the gravitational well of the neck region.

However, the $CO_2$ density was surprisingly low in the illuminated northern hemisphere during period B (many months before equinox), even if the surface temperature was sufficient to sublimate $CO_2$. This observation could be explained by the strong dichotomy between northern and southern surface features (El-Maarry et al. 2015): a thick dust layer could have been deposited from the last perihelion passage. During the short and intense southern summer, the ejected dust particles carried water ice towards the north. Such a dust layer would prevent the heat from penetrating deep enough to sublimate $CO_2$. However, it is not clear whether this interpretation can account for the change in $CO_2$ outgassing behaviour from period A to period B. The transition from period A, which still has significant $CO_2$ outgassing in the northern hemisphere (neck region), to period B, where it is essentially confined to the southern hemisphere, is even more visible when $CO_2$ density maps are analysed every month; there is a clear change around October and November 2014. The evolution of the dichotomy does not seem to be linked with orbitography variations: the distance was roughly stable with a slight increase during period B and the phase angle remained stabilized around 100 deg. An alternative interpretation for the low $CO_2$ and CO outgassing in the northern hemisphere before equinox (periods A and mostly B) could be related to the long summer period during which the northern hemisphere was illuminated. Far from the Sun, the temperature in the northern hemisphere may become sufficiently high to sublimate $CO_2$ but not $H_2O$ (the sublimation ice lines of $H_2O$ and $CO_2$ being approximately located at 2.6 AU and 20 AU, respectively), thus emptying the $CO_2$ reservoirs of the uppermost layers, whereas the southern hemisphere remains too cold to induce a significant sublimation of $CO_2$.

The diurnal skin depth and orbital skin depth of 67P are about a few centimeters and a few meters (Huebner et al. 2006), respectively. The $H_2O$ measured in the coma thus originates from the first centimeters below the surface of the comet, while $CO_2$ probably originates from layers located at a few meters maximum below the surface to allow for sufficient seasonal

driven heating, and probably at a few centimeters minimum to prevent a pure diurnal variability such as for $H_2O$. The same conclusions apply for CO and $CO_2$; CO, whose measurement interpretation is less easy owing to noise, has an even smaller diurnal variability, suggesting deeper sources in agreement with thermal models of comet nuclei.

## 4. Conclusions

We provide an analysis of the coma of comet 67P/Churyumov-Gerasimenko based on the ROSINA data from three periods between September 2014 and February 2016.

The influence of different parameters, such as illumination, distance spacecraft/comet, distance comet/Sun, sub-satellite point, nadir off-pointing angle, local time, and phase angle, on the outgassing detected by ROSINA was individually analysed and interpreted. As expected, the shape, attitude, and orbit directly impacts the sublimation of volatiles at the surface of the comet. Our observations reveal a strong difference of behaviour for the three main volatiles.

The analysis of RTOF data first confirms that outgassing of the main volatiles (water, carbon dioxide, and carbon monoxide) shows strong latitudinal and diurnal (longitude) variations. The $H_2O$ density was measured maximum above strongly illuminated areas (except the small lobe) including the active neck region before May 2015 equinox and moving slowly to the southern hemisphere after. The $CO_2$ outgassing was in general smaller than for $H_2O$ and was confined to the southern hemisphere (except before November 2014, where $CO_2$ and CO were detected above both hemispheres). The absence of $CO_2$ detection from the northern winter hemisphere early before the May 2015 equinox, despite a surface and subsurface temperature large enough to sublimate $CO_2$, suggests the presence of an icy dust layer covering the northern regions deposited after the previous perihelion, thus preventing the heat from reaching the $CO_2$ rich layers. This icy dust layer mainly contains water transported by the dust particles ejected from the southern hemisphere, leading to strong water outgassing during the northern summer hemisphere. Our observations (of $CO_2$ and, mostly, CO being more homogeneous than $H_2O$) are consistent with the assumption that $CO_2$ and CO originate from deeper layers than $H_2O$. Their sublimation is influenced by seasonal, diurnal, and surface heterogeneities effects.

Our study provides the first global comparison between the data recorded by the three instruments of ROSINA: DFMS, RTOF, and COPS. The comparison between those in situ data and the DSMC modelling reveals a very good correlation and understanding of the global behaviour of the main volatiles.

We analysed spectra during a large period of time, allowing the analysis of the relative dynamics of the three main volatiles and the displacement of the active regions for each species, especially after crossing the ice line and the May 2015 equinox. From our work, we conclude that the observed dynamic results from a complex combination of seasonal, diurnal, and surface heterogeneity effects.

*Acknowledgements.* The authors thank the following institutions and agencies, which supported this work: Work at IRAP was supported by the French space agency CNES. Work at the University of Bern was funded by the State of Bern, the Swiss National Science Foundation, and the European Space Agency PRODEX Programme. Work at the Max Planck Institute for Solar System Research was funded by the Max-Planck Society and Bundesministerium für Wirtschaft und Energie under contract 50QP1302. Work at the Southwest Research Institute was funded by NASA JPL. The results from ROSINA would not be possible without the work of the many engineers, technicians, and scientists involved in the mission, the Rosetta spacecraft, and the ROSINA instrument team over the past 20 yr, whose contributions are gratefully acknowledged. Rosetta is an European Space Agency (ESA) mission with contributions from its member states and NASA. We thank herewith the work of the whole ESA Rosetta team. All ROSINA flight data have been or will be released to the PSA archive of ESA and to the PDS archive of NASA.

## References

A'Hearn, M. F., Belton, M. J., Delamere, W. A., et al. 2011, Science, 332, 1396
Alí-Lagoa, V., Delbo', M., & Libourel, G. 2015, ApJ, 810, L22
Balsiger, H., Altwegg, K., Bochsler, P., et al. 2007, Space Sci. Rev., 128, 745
Bieler, A., Altwegg, K., Balsiger, H., et al. 2015, A&A, 583, A7
Biver, N., Hofstadter, M., Gulkis, S., et al. 2015, A&A, 583, A3
Bockelée-Morvan, D., Debout, V., Erard, S., et al. 2015, A&A, 583, A6
Bockelée-Morvan, D., Crovisier, J., Erard, S., et al. 2016, MNRAS, 462, S170
Capaccioni, F., Coradini, A., Filacchione, G., et al. 2015, Science, 347, 0628
De Sanctis, M., Lasue, J., Capria, M., et al. 2010, Icarus, 207, 341
De Sanctis, M., Capaccioni, F., Ciarniello, M., et al. 2015, Nature, 525, 500
El-Maarry, M., Thomas, N., Giacomini, L., et al. 2015, A&A, 583, A26
El-Maarry, M. R., Thomas, N., Gracia-Berná, A., et al. 2016, A&A, 593, A110
Feldman, P. D., A'Hearn, M. F., Bertaux, J.-L., et al. 2015, A&A, 583, A8
Filacchione, G., Capaccioni, F., Ciarniello, M., et al. 2016, Icarus, 274, 334
Fougere, N., Altwegg, K., Berthelier, J.-J., et al. 2016, A&A, 588, A134
Gasc, S. 2015, Ph.D. Thesis, Universitaet Bern, Switzerland
Gasc, S., Altwegg, K., Jäckel, A., et al. 2017, Planet. Space Sci.
Gulkis, S., Allen, M., von Allmen, P., et al. 2015, Science, 347, 0709
Hansen, K. C., Altwegg, K., Berthelier, J.-J., et al. 2016, MNRAS, 2413
Hässig, M., Altwegg, K., Balsiger, H., et al. 2015, Science, 347, 0276
Huebner, W. F., Benkhoff, J., Capria, M.-T., et al. 2006, Heat and gas diffusion in comet nuclei (International Space Science Institute)
Lee, S., Von Allmen, P., Allen, M., et al. 2015, A&A, 583, A5
Luspay-Kuti, A., Hässig, M., Fuselier, S., et al. 2015, A&A, 583, A4
Mall, U., Altwegg, K., Balsiger, H., et al. 2016, ApJ, 819, 126
Prialnik, D., Benkhoff, J., & Podolak, M. 2004, in Comets II (Tucson: Univ. of Arizona), 1, 359
Scherer, S., Altwegg, K., Balsiger, H., et al. 2006, Int. J. Mass Spectr., 251, 73
Sierks, H., Barbieri, C., Lamy, P. L., et al. 2015, Science, 347, 1044
Snodgrass, C., Tubiana, C., Bramich, D., et al. 2013, A&A, 557, A33
Vincent, J.-B., Bodewits, D., Besse, S., et al. 2015, Nature, 523, 63
Vincent, J.-B., Oklay, N., Pajola, M., et al. 2016, A&A, 587, A14

## Appendix A: Additional figures

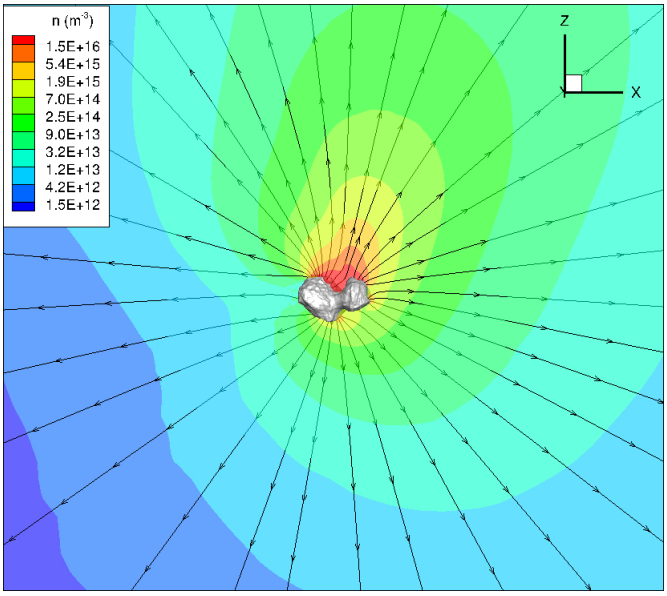


**Fig. A.1.** Simulation of density ($n$) and streamlines for 23 December 2014 at 12:00:00 UT from the model of Fougere et al. (2016).

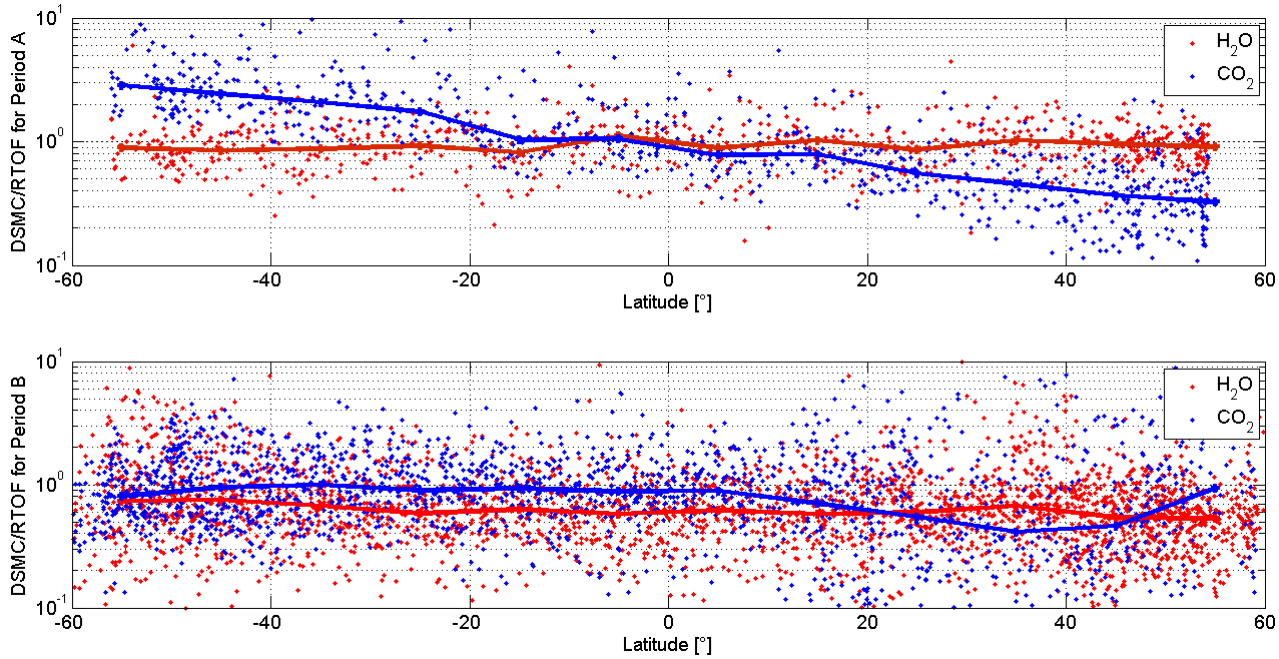


**Fig. A.2.** DSMC/RTOF ratio for $H_2O$ and $CO_2$ for Period A (*upper panel*) and Period B (*lower panel*).

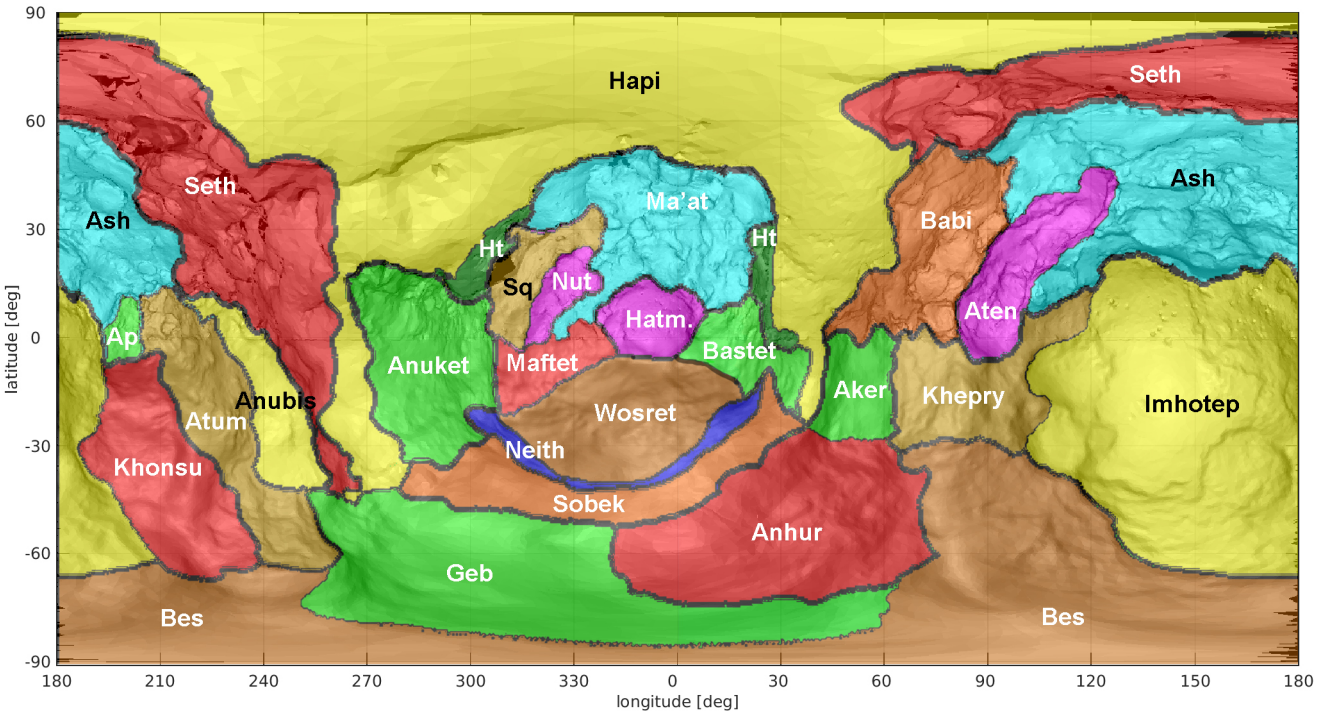


**Fig. A.3.** Two-dimensional longitude/latitude representation of the morphological regions defined by El-Maarry et al. (2016).

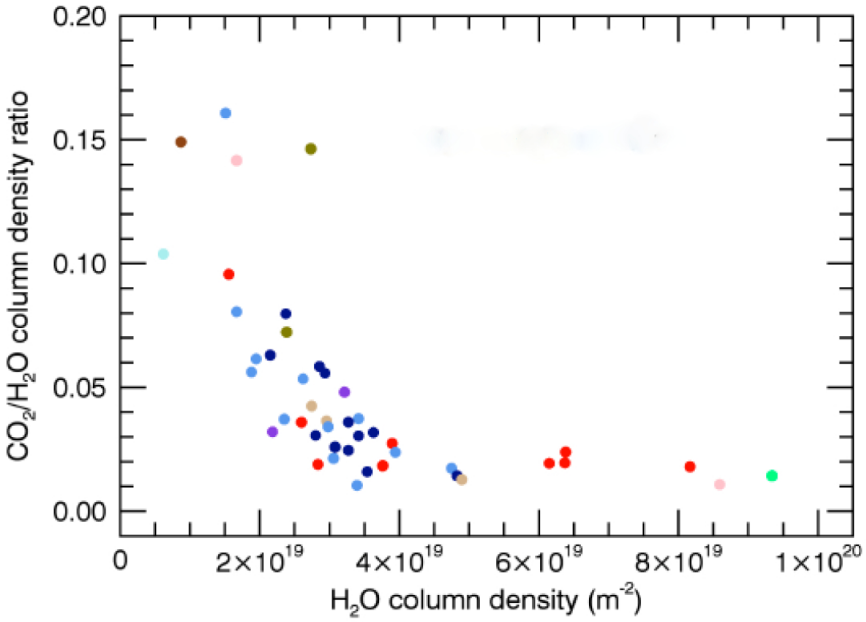


**Fig. A.4.** $CO_2/H_2O$ density ratio as a function of $H_2O$ density from Bockelée-Morvan et al. (2015), obtained from 24 November 2014 to 24 January 2015.